The Astrophysical Journal, 691:L133–L137, 2009 February 1 doi:10.1088/0004-637X/691/2/L133

VELOCITY-DEPENDENT CATASTROPHIC DISRUPTION CRITERIA FOR PLANETESIMALS

Sarah T. Stewart[1] and Zoë M. Leinhardt[2]
[1] Department of Earth and Planetary Sciences, Harvard University, 20 Oxford Street, Cambridge, MA 02138, USA; sstewart@eps.harvard.edu
[2] Department of Applied Mathematics and Theoretical Physics, Cambridge University, Cambridge CB3 0WA, UK; z.m.leinhardt@damtp.cam.ac.uk
Received 2008 October 16; accepted 2008 December 19; published 2009 January 15

ABSTRACT

The resistance of planetesimals to collisional erosion changes dramatically during planet formation. The transition between accretion and erosion from a collision is defined by the relationship between the mass of the largest remnant ($M_{\rm lr}$) and the normalized specific impact energy (Q/Q^*_D), where Q^*_D are the size-dependent catastrophic disruption criteria (the Q required to disperse half the target mass). Here, we calculate Q^*_D for gravitationally bound aggregates subject to low-velocity collisions (1–300 m s^{-1}) and compare the results to previous work at high velocities. We find that Q^*_D varies by orders of magnitude depending on the impact velocity and material properties. We define new variables to describe catastrophic disruption that remove ambiguities (over material density and projectile-to-target mass ratio) that are inherent in the traditional variables (Q and target radius): R_{C1} is the spherical radius of the combined projectile and target masses ($M_{\rm tot}$) at a density of 1 g cm^{-3}, Q_R is $0.5\mu V_{\rm i}^2/M_{\rm tot}$ (μ is the reduced mass and $V_{\rm i}$ is the impact velocity), and Q^*_{RD} is the Q_R required to disperse half the combined mass. We derive a universal law for the largest remnant, $M_{\rm lr}/M_{\rm tot} = -0.5(Q_R/Q^*_{RD} - 1) + 0.5$, and velocity-dependent catastrophic disruption criteria for strong and weak planetesimals for use in numerical studies of planet formation. Weak aggregate bodies are easily disrupted due to efficient momentum coupling during low-velocity collisions. Collisional growth of planetesimals requires a dynamically cold environment; alternatively, a noncollisional mechanism is required to form planetesimals large enough to be resistant to collisional disruption (several tens of kilometers).

Key words: comets: general – Kuiper Belt – minor planets, asteroids – solar system: formation

1. INTRODUCTION

The criteria for coagulation or fragmentation of planetesimals are a central component to understanding the accretion and collisional evolution of the solar system (e.g., Wetherill & Stewart 1993; Kenyon & Luu 1999; Leinhardt et al. 2000). Impact fragmentation studies have derived criteria for catastrophic disruption: the kinetic energy of the projectile per unit mass of the target such that half the target mass remains intact (Q^*_S; e.g., Fujiwara et al. 1989; Holsapple 1994; Holsapple et al. 2002). The criteria are size dependent and divided into two regimes: the collision outcome is dominated by decreasing tensile strength with size for smaller bodies and strengthening by self-gravity with size for larger bodies (Housen & Holsapple 1990) (curves in Figure 1(A)). In the gravity regime, the impact energy required to shatter a body (Q^*_S) is much less than the energy required to gravitationally disperse half the mass (Q^*_D; Melosh & Ryan 1997), and the largest remnant is a gravitationally reaccumulated rubble pile. In the strength regime, $Q^*_D = Q^*_S$, and the largest remnant is a single fragment.

Simulations of planet formation have implemented simplified rules, based on fragmentation studies, which govern the outcome of collisions. Currently available Q^*_D curves are primarily applicable to hypervelocity impacts, where a shock wave is generated, and impact scenarios where the projectile is much smaller than the target. However, in the early protoplanetary disk, relative velocities between planetesimals were very low (several m s^{-1} for km-scale bodies, e.g., Lissauer 1993; Wetherill & Stewart 1993), and the most energetic collisions were between comparable mass bodies. In addition, most previous studies have focused on nonporous bodies, whereas the first planetesimals were weak, porous aggregates (e.g., Whipple 1950; Weidenschilling 1997).

Here, we investigate the variability in disruption criteria under the wide range of conditions expected during planet formation and subsequent collisional and dynamical evolution. We expect significant changes in the collision outcome as (1) impact velocities increase from an elastic/plastic deformation regime to a shock regime (at hundreds of m s^{-1}), (2) initially porous planetesimals compact and differentiate, and (3) solid bodies are disrupted into rubble piles. In each case, the coupling of the projectile's energy and momentum into the target changes, altering the disruption criteria (Leinhardt et al. 2008).

We conduct numerical experiments of catastrophic disruption of gravitationally bound aggregates at low velocities by equal- and small-mass projectiles. Based on this work and previously published results, we propose a new definition for catastrophic disruption and derive criteria for the transition between accretion and erosion. Finally, we discuss the implications for collisionally driven planet formation.

2. METHODS

Low-velocity (1–300 m s^{-1}) collisions are modeled with PKDGRAV, an N-body gravity code (Richardson et al. 2000; Leinhardt et al. 2000; Stadel 2001; Leinhardt & Richardson 2002). Targets and projectiles are gravitational aggregates of rigid spheres (macroporous rubble piles; see the definition of macro- and microporosity in Section 3), with a bulk density range of 0.5–3.0 g cm^{-3}, spanning the measured densities of comets, asteroids, and trans-Neptunian objects. Each target contained ∼2500 particles, with porosity between 30% and 40%. Inelastic collisions between spheres are governed by a normal restitution coefficient of 0.2–0.8 (nominal value of 0.5) and no surface friction (Chau et al. 2002). We consider collisions onto 1, 10, and 50 km radii bodies by equal mass and small ($M_{\rm p}/M_{\rm targ} = 0.03$) projectiles to determine the effect of the projectile-to-target mass ratio on Q^*_D. In one case, the projectile is 1.5 times more massive than a 10 km radius target for illustrative purposes. We also include the results at $R_{\rm targ} = 1$ km from Leinhardt et al. (2000) (a similar data point was found by Korycansky & Asphaug 2006). The bodies have no

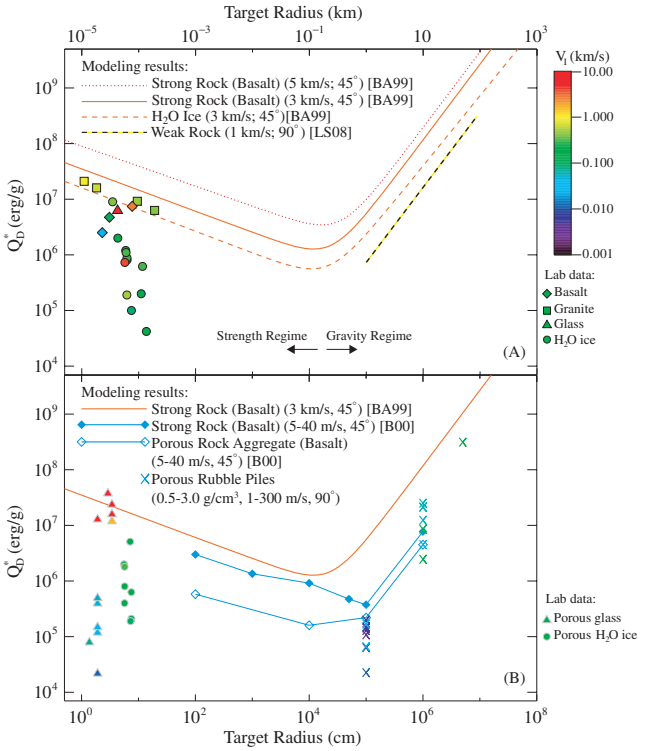

Figure 1. Traditional catastrophic disruption criteria (Q^*_D) as a function of target radius. Color denotes impact velocity. (A) Nonporous materials: numerical (Benz & Asphaug 1999; Leinhardt & Stewart 2009) and laboratory experiments (see the text). (B) Porous materials: laboratory data on glass and ice (see the text) and numerical experiments on aggregate rock (Benz 2000) and rubble piles (this work). High- and low-velocity Q^*_D for nonporous basalt are shown for reference.

initial spin, and the impact angle is 90°, producing Q^*_D values ∼10% less than 45° impacts (Leinhardt et al. 2000; Benz & Asphaug 1999).

Various numerical techniques have been used to model hypervelocity catastrophic disruption (Love & Ahrens 1996; Benz & Asphaug 1999; Benz 2000; Michel et al. 2001; Leinhardt & Stewart 2009). Hypervelocity disruption criteria (Figure 1(A)) have been calculated for strong rock, ice, and weak rock (nonporous rock with low shear strength; e.g., a compacted breccia). Here, we utilize very general definitions for strong and weak bodies. Strong bodies (with high shear and tensile strength) are primarily composed of crystalline rock, and weak bodies are composed of pure ices or aggregates (porous or nonporous) of ice and/or rock. Low-velocity disruption criteria have been calculated for strong rock and a 50% macroporous rock aggregate (Figure 1(B)). In the low-velocity cases, both the projectile mass and velocity were varied; some projectile masses were comparable to or larger than the target mass. Note that the different computational methods yield similar results for similar impact scenarios.

In the strength regime, laboratory fragmentation experiments have been conducted on a much wider range of materials. We consider basalt (Takagi et al. 1984), granite (Housen & Holsapple 1999), soda lime glass (Gault & Wedekind 1969), microporous soda lime glass (5%–60% porosity; Love et al. 1993; Setoh et al. 2007b), ice (Cintala et al. 1985; Kawakami et al. 1983; Lange & Ahrens 1987; Arakawa 1999; Arakawa et al. 1995; Giblin et al. 2004; Ryan et al. 1999; Kato et al. 1992, 1995), and micro and macroporous ice (10%–55%; Arakawa et al. 2002; Giblin et al. 2004) (symbols in Figure 1). Porous glass and ice targets are variably sintered aggregates of spherical glass beads and irregular ice chips, respectively. Target shapes vary; the data are plotted using radii of spheres of equal mass and density. In some cases, the critical disruption energy was refit (resulting in small differences on the scale of Figure 1) by the authors using a linear relationship between the largest fragment and the impact energy (see below). One point from Setoh et al. (2007c) lies off the figure at $R_{\rm targ} = 1.9$ cm and $Q^*_D = 300$ erg g^{-1}. Symbol colors denote the critical impact velocity that corresponds to the value of Q^*_D for the projectile mass used in the experiment (in all cases except the lowest value for basalt, $M_{\rm p} \ll M_{\rm targ}$). Most of the laboratory data are in the shock regime; a subset of the data on basalt (one point) and porous glass (seven points including one off scale) have critical impact velocities less than 100 m s^{-1}.

3. RESULTS

The catastrophic disruption criteria span five orders of magnitude for bodies with sizes up to protoplanets (∼1000 km, Figure 1). The criteria are sensitive to factors that influence the energy and momentum coupling between projectile and target (e.g., impact velocity, projectile-to-target mass ratio, and material properties such as strength and porosity), which are expected to vary significantly during the formation and collisional evolution of planets. Several general trends can be drawn from the data.

In nonporous materials (Figure 1(A)), the laboratory-scale disruption criteria are controlled primarily by tensile strength. For example, strong rocks (basalt, granite) have a larger disruption criteria than average ice. The scatter in the ice data reflects differences in sample preparation (strength), projectile material, velocity, and temperature. Note that the results from numerical experiments on ice are about an order of magnitude larger than the average ice data (∼10^6 erg g^{-1} at 6 cm). In the gravity regime, shear strength (weak versus strong nonporous rock) has a smaller but noticeable effect on the disruption criteria (factors of few to several; Leinhardt & Stewart 2009). In addition, based on theory (Housen & Holsapple 1990) and numerical experiments, the disruption criteria increase with increasing impact velocity as more energy is partitioned into shock deformation (3 km s^{-1} versus 5 km s^{-1} strong rock curves).

The disruption of porous materials is more complicated. Hypervelocity laboratory experiments in porous ice and porous glass, which are mechanically weak, require similar or larger impact energies for disruption compared to their mechanically stronger solid counterparts (circles and triangles in Figure 1(A) versus Figure 1(B)). Porous materials are efficient shock absorbers, and the projectile energy is inefficiently coupled to the target, requiring larger impact energies for disruption. Note that the outcome may also depend on the scale of the porosity: voids smaller than the thickness of the shock front are compacted by the shock (microporous), whereas the shock wave reflects off larger void spaces (macroporous) (see Leinhardt et al. 2008). At extremely low impact velocities (less than 100 m s^{-1}), numerical (this work and Benz 2000) and laboratory (porous glass data from Setoh et al. 2007a, 2007c) disruption criteria are significantly smaller than the hypervelocity case for both solid and porous bodies (basalt and glass in Figure 1). In this case, momentum coupling is more efficient because of a combination of larger projectile sizes and no shock deformation (e.g., melting). In the low-velocity strength regime, the catastrophic disruption criteria are still dependent on strength; however, the Q^*_D values

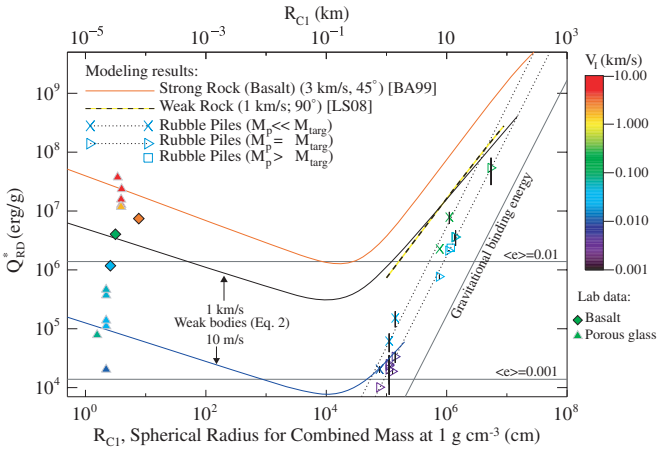

Figure 2. New reduced mass catastrophic disruption criteria (Q^*_{RD}) vs. R_{C1}. In this space, low-velocity rubble pile results fall onto two lines (dotted): one for $M_p = M_{targ}$ and one for $M_p \ll M_{targ}$ (with 1σ error bars). Horizontal lines denote impact energy for equal-mass colliding bodies with mean eccentricities of 0.01 and 0.001 at 30 AU.

are reduced by orders of magnitude compared to hypervelocity impacts on porous targets with the same material strength (see discussion in Setoh et al. 2007a, 2007c). Numerical experiments of hypervelocity collisions onto microporous bodies are currently in development (e.g., Jutzi et al. 2008). In the gravity regime, the disruption criteria may be comparable to solid bodies if the lower density (and hence lower gravity) trades off with the less efficient energy coupling.

The available data for 1 km radius bodies show that the disruption criteria may vary by an astounding three orders of magnitude from low-velocity collisions between rubble piles to hypervelocity collisions onto strong bodies (Figure 1(B)). The scatter in the rubble pile experiments reflects the differences in density and projectile-to-target mass ratio, which are not discerned by the traditional presentation of the catastrophic disruption criteria (Q^*_D versus R_{targ}). Hence, we propose a new definition for the disruption criteria that is more illuminating.

3.1. New Catastrophic Disruption Variables

We propose new variables to describe catastrophic disruption. The original definition uses the target radius, R_{targ}, and the specific impact energy, $Q = 0.5 M_p V_i^2 / M_{targ}$, where M_p is the mass of the projectile, V_i is the impact velocity, and M_{targ} is the mass of the target. The criterion for catastrophic disruption by shattering (Q^*_S; or gravitational dispersal, Q^*_D) is the value of Q where the mass of the largest single fragment (or gravitationally re-accumulated remnant), M_{lr}, equals half the target mass.

In order to account for the mass of the projectile and the density of the bodies, we use the variables R_{C1} and Q_R. R_{C1} is the spherical radius of the combined projectile and target mass at a density of 1 g cm^{-3}. Q_R is the reduced mass kinetic energy scaled by the total mass of the colliding system, $0.5 \mu V_i^2 / M_{tot}$, where $\mu = M_p M_{targ} / M_{tot}$ and $M_{tot} = M_p + M_{targ}$. The critical energies for shattering and gravitational dispersal, Q^*_{RS} and Q^*_{RD}, respectively (recommended pronunciation: Q-stars and Q-starred), are defined as the value of Q_R where $M_{lr} = 0.5 M_{tot}$.

Some of the data are replotted in the new variable space in Figure 2. The rubble pile results fall onto two lines (dotted), one for $M_p \ll M_{targ}$ and one for $M_p = M_{targ}$, given by $Q^*_{RD} = a R_{C1}^2$ (cgs). For the equal-mass bodies, $a = 1.7 \pm 0.3 \times 10^{-6}$, which is about 10 times larger than the gravitational binding energy of the combined bodies (Leinhardt et al. 2000). For $M_p \ll M_{targ}$, $a = 5.3 \pm 1.8 \times 10^{-6}$. Thus, the catastrophic disruption criteria for the small projectile case are about three times larger than the equal-mass case; the difference is a result of the less-efficient coupling of momentum by a small projectile compared to an equal-sized projectile. The strengthless equal-mass case defines the lower limit for disruption by any impact event in the gravity regime.

In the new variable space, the different densities of the rubble piles are accounted for by the normalized size, R_{C1}. The cluster of equal-mass points at $R_{C1} = 1$ km reflects insignificant variations from changes in the normal coefficient of restitution (ranging from 0.2 to 0.8). In the gravity regime, the catastrophic disruption criteria are controlled by the impact-generated mass–velocity distribution and not affected by the details of the re-accumulation process (see also Leinhardt & Stewart 2009). The coefficient of restitution may be more important in cases of fast pre-impact spin or highly grazing impacts.

For rubble piles, the critical velocities for catastrophic disruption (V^*_{RD}) scales linearly with size, ranging from 3 to 254 m s^{-1} in Figure 2. We fit $V^*_{RD} = b R_{C1}$ (cgs), where $b = 0.0037 \pm 0.0003$ for equal-mass projectiles and $b = 0.020 \pm 0.003$ for small projectiles. The critical velocity defines the lower limit for catastrophic disruption; collisions at slower speeds will result in a remnant larger than $0.5 M_{tot}$ (net growth for equal-mass bodies). In other words, catastrophic disruption at velocities below V^*_{RD} on the equal-mass line requires a projectile mass larger than the target.

In the new variable space (Figure 2), $Q^*_{RD} \sim Q^*_D$ for hypervelocity impacts by small projectiles and the target radius must be converted to R_{C1}. In the gravity regime, only some of the difference between the disruption criteria for basalt and ice at 3 km s^{-1} is removed using the new variables, reflecting the influence of other material properties. The slope of the 3 km s^{-1} basalt disruption curve (and the ice curve, not shown) shallows for the largest bodies because the projectile mass becomes a significant fraction of the target mass.

3.2. A Universal Law for the Largest Remnant Mass

The relationship between the mass of the largest postcollision remnant and the impact energy defines the conditions for net accretion versus net erosion. The mass of the largest fragment normalized to the target mass scales linearly with the impact energy normalized by Q^*_D over an extremely wide range of impact conditions in both laboratory and numerical experiments (see Housen & Holsapple 1990 for a discussion of the linearity). However, the slope of the fit depends on the projectile-to-target mass ratio (Figure 3(A)). The linear slope is about -0.5 for both hypervelocity and low-velocity collisions with $M_p \ll M_{targ}$ in solid and porous materials (e.g., this work and Benz & Asphaug 1999; Leinhardt & Stewart 2009; Takagi et al. 1984; Gault & Wedekind 1969; Setoh et al. 2007b). For equal-mass rubble piles, the mass of the largest remnant is greater than the target (net accretion) for impact energies less than 70% of Q^*_D; hence, there is a very rapid transition between net accretion and catastrophic disruption. For $M_p > M_{targ}$ rubble piles, the slope steepens as the mass of the projectile increases.

Using the new variables for catastrophic disruption, the dependence on projectile-to-target mass ratio is removed (Figure 3(B)). The mass of the largest remnant follows a single

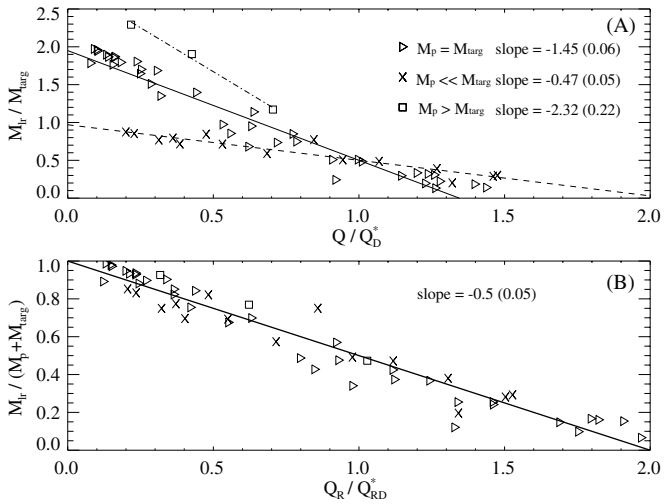

Figure 3. Mass of the largest remnant vs. impact energy. (A) Traditional variables. Symbols are low-velocity rubble pile results. In this space, the slope of the linear relationship depends on the projectile-to-target mass ratio. Hypervelocity data follow the $M_p \ll M_{targ}$ line (dashed). (B) New variables for catastrophic disruption. The −0.5 slope linear relationship (Equation 1) is a universal result for all catastrophic impact conditions. 1σ errors are given in parenthesis.

linear relationship:

$$M_{lr}/M_{tot} = -0.5(Q_R/Q^*_{RD} - 1) + 0.5, \quad (1)$$

for $0 < Q_R/Q^*_{RD} < 2$. This relationship is universal and applies in both the strength and gravity regime and for nonporous and porous materials.

The universal relationship does not hold for conditions that depart from the catastrophic disruption regime. At very low impact velocities, large bodies will merge completely under gravitational forces and small bodies will transition from fragmentation to rebounding to sticking. In the supercatastrophic regime ($Q_R/Q^*_{RD} > 2$), the relationship becomes a power law (e.g., Takagi et al. 1984).

4. IMPLICATIONS FOR PLANET FORMATION

Here, we demonstrate that the catastrophic disruption criteria change by orders of magnitude depending on impact velocity and mechanical properties. This work validates the results from Benz (2000) and expands upon his conclusions. The critical impact velocity required to begin collisional erosion of weak aggregate bodies is only a few m s^{-1}. Therefore, the transition from the coagulation phase to collisional erosion for km-sized bodies begins much earlier during planet formation than usually considered. Our result that km-scale aggregates are particularly susceptible to disruption is supported by the observed deficit of small bodies ($\lesssim$1 km) in the outer solar system (Bierhaus et al. 2005; Meech et al. 2004).

During planet formation, relative impact velocities increase as a result of several effects: e.g., dispersal of the nebular gas, formation of protoplanets, and migration of giant planets. As impact velocities rise, the catastrophic disruption criteria also increases. The data on the velocity dependence in the strength regime are complicated by differences in strength; however, there is clear evidence for a sharp increase in Q^*_{RD} between tens of m s^{-1} and a couple of km s^{-1} for porous materials (Figure 1(B) and Setoh et al. 2007b). In the gravity regime, the data (using two different numerical techniques) on weak bodies display a more systematic dependence on velocity (Figure 2).

Further work is required to robustly link the strength and gravity regimes for weak aggregate bodies. Meanwhile, we suggest that the samples of sintered glass beads are the best laboratory analog for gravitational rubble piles (e.g., near-Earth asteroid Itokawa; Fujiwara et al. 2006). Although the mechanical properties of planetesimals are not well understood, theory and observations of comets suggest that their strength is extremely low (Sirono & Greenberg 2000; Richardson et al. 2007; Asphaug & Benz 1996) and lower than the strength of samples in the porous glass experiments.

Following Housen & Holsapple (1990, 1999), we present velocity-dependent catastrophic disruption curves of the form

$$Q^*_{RD} = q_s R_{C1}^{9\mu/(3-2\phi)} V_i^{2-3\mu} + q_g R_{C1}^{3\mu} V_i^{2-3\mu}, \quad (2)$$

where μ and ϕ are material properties and density is not included in the gravity term (right) because of the definition of R_{C1}. To derive constants for weak aggregates, we fit the weak rock hypervelocity data and rubble pile low-velocity data in the gravity regime and the porous glass data in the strength regime. We find that $\mu = 0.4$ (the value for sand; nearly pure momentum scaling), $\phi = 7$, $q_s = 500$, and $q_g = 10^{-4}$ (in cgs units) provide an excellent fit to the gravity regime data and a good fit to the laboratory data. The slope in the strength regime is determined by the flaw distribution parameter, ϕ, which is constrained to lie between 6 and 9 for many materials (see Housen & Holsapple 1999). The simple equation fits the data for weak aggregates over the entire velocity range of available data, from a few m s^{-1} to a few km s^{-1} (curves for 10 m s^{-1} and 1 km s^{-1} are shown in Figure 2). Note that the constant-velocity disruption criteria are truncated by the strengthless equal-mass line in the gravity regime, which defines the combined mass that cannot be dispersed at that velocity.

We also fit velocity-dependent catastrophic disruption curves for strong rocks (not shown) using the basalt laboratory data, which spans critical velocities from 33 to 2800 m s^{-1}, and the modeling results from Benz & Asphaug (1999). We find $\mu = 0.5$, $\phi = 8$, $q_s = 7 \times 10^4$, and $q_g = 10^{-4}$ provide a reasonable fit. The fitted coefficients describe generic materials over a wide range of impact conditions.

Planet formation simulations should maintain different fragmentation criteria for strong and weak bodies. When strong bodies are subject to nearly catastrophic events (in the gravity regime, shattered but not dispersed, $Q^*_{RS} < Q_R < Q^*_{RD}$; in the strength regime, $0.25Q^*_{RS} < Q_R < Q^*_{RS}$, see Housen 2009), the outcome of the next impact event will be determined by the weak aggregate disruption criteria. Future numerical simulations of planet formation should use Equations (1) and (2) to describe the outcome of collisions. In practice, the strength regime parameters q_s and ϕ should be varied to consider the possible range of material properties for planetesimals.

Our low-velocity catastrophic disruption criteria have major implications for planet formation. Collisional coagulation of planetesimals larger than ∼1 km must have occurred in a dynamically cold environment; alternatively, planetesimal growth was aided by a noncollisional mechanism such as gravitational instabilities and/or turbulence (Goldreich & Ward 1973; Johansen et al. 2007; Cuzzi et al. 2008).

The catastrophic disruption criteria for bodies smaller than ∼100 km change dramatically during the formation and evolution of the solar system. Kilometer-sized planetesimals are easily disrupted by collisions; hence, mechanisms that lead to rapid formation of planetesimals large enough to be resistant to collisions (several tens of kilometers) are required.

We thank P. Michel (reviewer), J. Cuzzi, K. Housen, and S. Kenyon for useful discussions and feedback. This work was supported by NASA grant NNG05GH46G and an STFC fellowship (Z.M.L.).

REFERENCES

Arakawa, M. 1999, Icarus, 142, 34
Arakawa, M., Leliwa-Kopystynski, J., & Maeno, N. 2002, Icarus, 158, 516
Arakawa, M., Maeno, N., Higa, M., Iijima, Y., & Kato, M. 1995, Icarus, 118, 341
Asphaug, E., & Benz, W. 1996, Icarus, 121, 225
Benz, W. 2000, Space Sci. Rev., 92, 279
Benz, W., & Asphaug, E. 1999, Icarus, 142, 5
Bierhaus, E. B., Chapman, C. R., & Merline, W. J. 2005, Nature, 437, 1125
Chau, K. T., Wong, R. H. C., & Wu, J. J. 2002, Int. J. Rock Mech. Min. Sci., 39, 69
Cintala, M. J., Horz, F., Smrekar, S., & Cardenas, F. 1985, Lunar Planet. Sci. Conf. 16, 129
Cuzzi, J. N., Hogan, R. C., & Shariff, K. 2008, ApJ, 687, 1432
Fujiwara, A., Cerroni, P., Davis, D., Ryan, E., Di Martino, M., Holsapple, K., & Housen, K. 1989, in Asteroids II, ed. R. P. Binzel, T. Gehrels, & M. S. Matthews (Tucson, AZ: Univ. Arizona Press), 240
Fujiwara, A., et al. 2006, Science, 312, 1330
Gault, D. E., & Wedekind, J. A. 1969, J. Geophys. Res., 74, 6780
Giblin, I., Davis, D. R., & Ryan, E. V. 2004, Icarus, 171, 487
Goldreich, P., & Ward, W. R. 1973, ApJ, 183, 1051
Holsapple, K. A. 1994, Planet. Space Sci., 42, 1067
Holsapple, K. A., Giblin, I., Housen, K. R., Nakamura, A., & Ryan, E. V. 2002, in Asteroids III, ed. W. Bottke, Jr., A. Cellino, P. Paolicchi, & R. Binzel (Tucson, AZ: Univ. Arizona Press), 443
Housen, K. 2009, Planet. Space Sci. in press
Housen, K. R., & Holsapple, K. A. 1990, Icarus, 84, 226
Housen, K. R., & Holsapple, K. A. 1999, Icarus, 142, 21
Johansen, A., Oishi, J. S., Mac Low, M. M., Klahr, H., & Henning, T. 2007, Nature, 448, 1022
Jutzi, M., Benz, W., & Michel, P. 2008, Icarus, 198, 242
Kato, M., Iijima, Y., Arakawa, M., Okimura, Y., Fujimura, A., Maeno, N., & Mizutani, H. 1995, Icarus, 113, 423
Kato, M., Iijima, Y., Okimura, Y., Arakawa, M., Maeno, N., Fujimura, A., & Mizutani, H. 1992, in Physics and Chemistry of Ice, ed. N. Maeno & T. Hondoh (Sapporo: Hokkaido Univ. Press), 464
Kawakami, S., Mizutani, H., Takagi, Y., Kato, M., & Kumazawa, M. 1983, J. Geophys. Res., 88, 5806
Kenyon, S. J., & Luu, J. X. 1999, AJ, 118, 1101
Korycansky, D. G., & Asphaug, E. 2006, Icarus, 181, 605
Lange, M. A., & Ahrens, T. J. 1987, Icarus, 69, 506
Leinhardt, Z. M., & Richardson, D. C. 2002, Icarus, 159, 306
Leinhardt, Z. M., Richardson, D. C., & Quinn, T. 2000, Icarus, 146, 133
Leinhardt, Z. M., & Stewart, S. 2009, Icarus, in press
Leinhardt, Z. M., Stewart, S. T., & Schultz, P. H. 2008, in The Solar System Beyond Neptune, ed. A. Barucci, H. Boehnhardt, D. Cruikshank, & A. Morbidelli (Tucson, AZ: Univ. Arizona Press), 195
Lissauer, J. J. 1993, ARA&A, 31, 129
Love, S. G., & Ahrens, T. J. 1996, Icarus, 124, 141
Love, S. G., Hörz, F., & Brownlee, D. E. 1993, Icarus, 105, 216
Meech, K. J., Hainaut, O. R., & Marsden, B. G. 2004, Icarus, 170, 463
Melosh, H. J., & Ryan, E. V. 1997, Icarus, 129, 562
Michel, P., Benz, W., Tanga, P., & Richardson, D. C. 2001, Science, 294, 1696
Richardson, J. E., Melosh, H. J., Lisse, C. M., & Carcich, B. 2007, Icarus, 190, 357
Richardson, D. C., Quinn, T., Stadel, J., & Lake, G. 2000, Icarus, 143, 45
Ryan, E. V., Davis, D. R., & Giblin, I. 1999, Icarus, 142, 56
Setoh, M., Hiraoka, K., Nakamura, A. M., Hirata, N., & Arakawa, M. 2007a, Adv. Space Res., 40, 252
Setoh, M., Nakamura, A. M., Hiraoka, K., Onose, N., Hasegawa, S., & Michel, P. 2007b, in Lunar Planet. Sci. Conf. 38, Abs. 1263
Setoh, M., Nakamura, A. M., Hirata, N., Hiraoka, K., & Arakawa, M. 2007c, Earth Planets Space, 59, 319
Sirono, S., & Greenberg, J. M. 2000, Icarus, 145, 230
Stadel, J. G. 2001, PhD thesis, Univ. Washington, Seattle
Takagi, Y., Mizutani, H., & Kawakami, S. 1984, Icarus, 59, 462
Weidenschilling, S. J. 1997, Icarus, 127, 290
Wetherill, G. W., & Stewart, G. R. 1993, Icarus, 106, 190
Whipple, F. L. 1950, ApJ, 111, 375